Pharmaceutical Research, Vol. 26, No. 2, February 2009 (© 2008)
DOI: 10.1007/s11095-008-9745-6

Research Paper

Investigating the Movement of Intravitreal Human Serum Albumin Nanoparticles in the Vitreous and Retina

Hyuncheol Kim,[1,2] Shaun B. Robinson,[1] and Karl G. Csaky[1]

Received June 29, 2008; accepted October 2, 2008; published online October 29, 2008

Purpose. To investigate the movement of intravitreally injected human serum albumin nanoparticles (HSA-NP) with respect to nanoparticle surface charge and retinal injury.
Methods. HSA-NPs were developed by a desolvation technique. HSA-NPs were cationized by covalent coupling of hexamethylenediamine on the particle surface. Either anionic or cationic HSA-NPs were injected to determine the effect of surface charge on intravitreal nanoparticle movement. HSA-NPs were injected intravitreally into both normal and laser photocoagulated eyes to examine the effect of the integrity of retinal tissue on the retinal penetration. The retinal penetration of fluorescence labeled anionic HSA-NPs was investigated by confocal microscopy.
Results. Anionic particles (−33.3±6.1 mV) more easily diffused through the 3-dimensional vitreal network of collagen fibrils than did their cationic counterparts (11.7±7.2 mV). In the laser photocoagulated retina, more HSA-NPs were detected in the choroidal space, compared to the normal retina. The immunohistochemical studies indicated that HSA-NPs were taken up into Müller cells.
Conclusions. The movement of intravitreal nanoparticles depended on both nanoparticles surface charge and retinal injury. The Müller cells might play an important role in the retinal penetration of nanoparticles. The anionic HSA-NP is a promising drug or gene delivery carrier to the sub-retinal space and RPE.

KEY WORDS: human serum albumin nanoparticles; Müller cells; trans-retinal penetration.

INTRODUCTION

Long-term delivery of therapeutic agents to the retina and retinal pigment epithelium (RPE) is limited and challenging because of several ocular barriers (1,2). Currently, intravitreal injection is the most efficient method used in the clinic to deliver drugs directly to the posterior segment of the eye (3). Although direct intravitreal injection has shown favorable results in clinical trials, the short half-life of this method necessitates frequent administration, which is accompanied by the risk of vitreous hemorrhage, retinal detachment, and/or endophthalmitis (4,5). Nano-sized drug delivery systems have been studied extensively to deliver therapeutic agents to the posterior segment of the eye for an extended period of time (6). However, the distribution and elimination of intra-ocularly administered nano-sized drug delivery systems is not yet well understood. Without understanding the factors influencing the distribution and elimination of nano-sized drug delivery particles in the eye, it is difficult to develop an optimized drug-delivery system to treat retinal diseases.

We sought to understand the movement of intravitreally administered nanoparticles in the vitreous and retina. Herein, we present the distribution of intravitreal nanoparticles, with respect to both nanoparticle surface charge and retina injury. Additionally, we introduce a possible mechanism for trans-retinal penetration of intravitreal nanoparticles into the sub-retinal space. We used a human serum albumin nanoparticle (HSA-NP) because it has been well studied for ocular drug delivery and showed excellent intraocular tolerance (7–9). Furthermore, the particles could be easily prepared under soft conditions, by coacervation or controlled desolvation processes (7).

METHODS

Animals

All procedures adhered to the guideline from the Association for Research in Vision and Ophthalmology for the Use of Animals in research, with approval from the Institutional Animal Care and Use Committee at Duke University.

Nanoparticle Preparation

The HSA-NPs were prepared by a previously described desolvation technique (10). Thirty milligrams of human serum albumin (Sigma, St. Louis, MO, USA) was dissolved in 5 mL

[1] Department of Ophthalmology, Duke University Medical Center, 2530 Erwin Rd. DUMC Box 3802, Durham, North Carolina 27705, USA.
[2] To whom correspondence should be addressed. (e-mail: hyuncheol.kim@duke.edu)

of pure water. Ethanol, 6.5 mL, was added dropwise to the human serum albumin solution and stirred for 1 h; 0.5 μL of 50% glutaraldehyde was added to the HSA-NP suspension and stirred overnight at room temperature. After 24 h of constant stirring, the resulting nanoparticles were purified by three times centrifugation (12,500 RPM, 55 min, at 4°C) and re-suspension with pure water. Finally, the particle suspension was centrifuged (3,000 RPM, 5 min, at 4°C) to remove aggregates.

Particle Analysis

Particle size was determined by photon correlation spectroscopy (PCS) using quasi-elastic light scattering equipment (ZetaPlus™ equipped with particle sizing mode, Brookhaven Instrument Crop., Holtsville, NY, USA). A dilute suspension of nanoparticles was prepared in distilled water. The sample was subjected to particle size analysis and analyzed in duplicate with ten readings per nanoparticle sample. Zeta potential of nanoparticles in distilled water was determined using ZetaPlus™ in the zeta potential analysis mode in duplicate with three readings per nanoparticle sample.

Preparation of Fluorescent Dye Conjugated HSA-NPs

One milligram of Alexa555 carboxylic acid succinimidyl ester (Invitrogen, Carlsbad, CA, USA) was dissolved in 100 μL of DMSO. 10 μL of the Alexa dye solution was added to 2 mL of HSA-NP suspension and stirred overnight without light. To remove non-conjugated Alexa dye from the solution, the particles were centrifuged (12,500 RPM, 55 min, at 4°C) and re-suspended three times. Both size and surface charge of the final product were determined as described above. Finally, particle aggregates were removed as described above.

Preparation of Cationic HSA-NPs

HSA-NPs were cationized by covalent coupling of ethylenediamine to carboxyl groups, as previously described (11). Briefly, 1 mL of 15 M ethylenediamine (Sigma, St. Louis, MO, USA) was added to 9 mL of anionic HSA-NP suspension. The pH of the solution was then adjusted to 7.8 with 1 N HCl. After stirring for 30 min at room temperature, 0.5 g of 1-ethyl-3-(3-dimethylaminopropyl) carbodiimide hydrochloride (Pierce Biotechnology, Rockford, IL, USA) was added and cationization was allowed to proceed at room temperature for 4 h. Excess reagent was removed by repeated centrifugation (12,500 RPM, 55 min, 4°C) and the particles were re-suspended with ultrapure water. Alexa 555 fluorescence dye was then conjugated to the cationized HSA-NP as described above. Both size and surface charge of the final product were also determined as described above.

Determination of the Retinal Distribution of Intravitreally Administered HSA-NPs

Two microliters of Alexa 555 conjugated HSA-NPs (3.3 mg/mL) were administered into the vitreous of rat eyes by a 32 gauge needle (Hamilton, Reno, NV, USA) under contact lens visualization. Five hours post intravitreal administration, the eyes were enucleated and fixed immediately with 4% paraformaldehyde solution (PFA). The eye was opened by circumferential incisions at the surgical limbus after overnight fixation. After removal of the anterior segment and lens, the posterior segment of the eye was embedded in 7% agarose type XI gel (Sigma, St. Louis, MO, USA) and sectioned into 150 μm-thick slices with a vibrating blade microtome (Leica, Bannockbum, IL, USA). The eye sections were incubated overnight in DAPI solution (1:1,000) diluted with ICC buffer and then washed three times with ICC buffer for 3 h. The eye sections were embedded in mounting medium (Vectashield, Vector Laboratories Inc., Burlingame, CA, USA) and sealed under microscope cover glass slides. The eye sections were viewed on a Leica laser scanning confocal microscope (Leica SP2, Carl Zeiss, Inc., Exton, PA, USA).

To determine the distribution of intravitreal HSA-NPs in the laser-coagulated retina, four laser burns between retinal vessels around the optic nerve head were induced by using the blue-green setting of a Lumenis Ultima Argon Laser (Lumenis Inc., New York, NY, USA). The laser power, duration, and spot diameter were 180-mW, 0.1 s, and 50-μm, respectively. Two weeks after the laser photocoagulation, 2 μL of Alexa 555 conjugated HSA-NPs were administered into the lasered eye. All procedures after the injection were same as the above.

Distribution of Intravitreally Administered Anionic *vs.* Cationic HSA-NP in Vitreous

Two microliters of Alexa 555 conjugated anionic (3.3 mg/mL) or cationic HSA-NPs (3.3 mg/mL) were administered intravitreally. Five hours post injection, the eyes were enucleated and fixed immediately with 4% PFA solution. One hundred fifty micrometer-thick slices were made as above described. These eye sections were viewed on an epifluorescence microscope (Zeiss Axiophot, Carl Zeiss, Inc., Exton, PA, USA). The average fluorescence intensities in the vitreous were determined with ImageJ. The statistical analysis between the anionic group and the cationic group was performed by *t*-test.

Immunohistochemistry

A rabbit anti-human von Willebrand factor antibody (DAKO, Carpinteria, CA, USA) (12) and a mouse anti-glutamine synthetase (CHEMICON International Inc., Temecula, CA, USA) (13) were utilized for Immunohistochemistry staining of retinal blood vessels and Müller cells, respectively. The 150 μm-thick eye sections were incubated in 5% goat serum overnight. Double staining was performed using rabbit anti-human von Willebrand factor antibody (dilution 1:150) and mouse anti-glutamine synthetase (dilution 1:150) with 2% goat serum ICC buffer as a primary antibody solution. The primary antibodies, anti-von Willebrand factor and anti-glutamine synthetase, were detected using a secondary antibody solution containing Alexa Fluor® 488 goat anti-rabbit IgG (dilution 1:150), Alexa Fluor® 633 goat anti-mouse IgG (dilution 1:150), and DAPI (dilution 1:1,000) in ICC buffer.

Table 1. Summary of Physical Properties of HSA-NPs Used in This Study

	Size (nm)	Zeta potential (mV)	Usage
Particle I	107.3±31.1	−23.73±3.03	Fig. 1
Particle II	114.0±10.1	−33.3±6.1	Fig. 2A
Particle III	175.5±16.4	11.7±7.2	Fig. 2B
Particle IV	125.1±29.6	−23.7±3.0	Fig. 3, 4, 5, and 6

Imaging Process

The distributions of intravitreal HSA-NPs in the whole vitreous and retina with respect to nanoparticles surface charge were determined by imaging the 150 μm-thick section using an epifluorescence microscope (Zeiss Axiophot, Carl Zeiss, Inc., Exton, PA, USA) with ×2.5 magnification and identical exposure times. Several images, which show the distribution of HSA-NPs in limited regions of the vitreous and retina, were combined into one image to show the overall distribution of HSA-NPs in the whole vitreous and retina with Adobe Photoshop software (version 7.0). The trans-retinal penetration of intravitreal HSA-NPs was demonstrated by projection of 30 confocal slide images (0.5-μm slide thickness per each image).

RESULTS

Particle Analysis

Table 1 summarizes physical properties of HSA-NPs used in this study. Plain HSA-NPs show 107.3±31.1 nm size distribution (Fig. 1A), and −23.73±3.03 mV zeta potential (Fig. 1B). Figure 1C shows an electron microscopy image demonstrating a spherical and uniform shape. After the conjugation of Alexa dyes, the average particle size increased slightly (particle II and IV in Table 1). The size and zeta potential of cationized HSA-NPs was determined to be 175.5± 16.4 and 11.7±7.2 mV, respectively.

Vitreal Penetration of Anionic *vs.* Cationic HSA-NP

Figure 2 shows the vitreal distribution of cationic HSA-NP (A) and anionic HSA-NP (B) 5 h post intravitreal administration. Most of intravitreal cationic HSA-NPs were filtered and could not penetrate the vitreous ($p=0.005$). Most of intravitreal anionic HSA-NPs penetrated the vitreous and were located within the retina at 5 h. Anionic HSA-NPs penetrated the vitreal barrier more easily than cationic HSA-NPs possibly due to electrostatic attraction between cationic HSA-NPs and the negatively charged vitreal glycosaminoglycan.

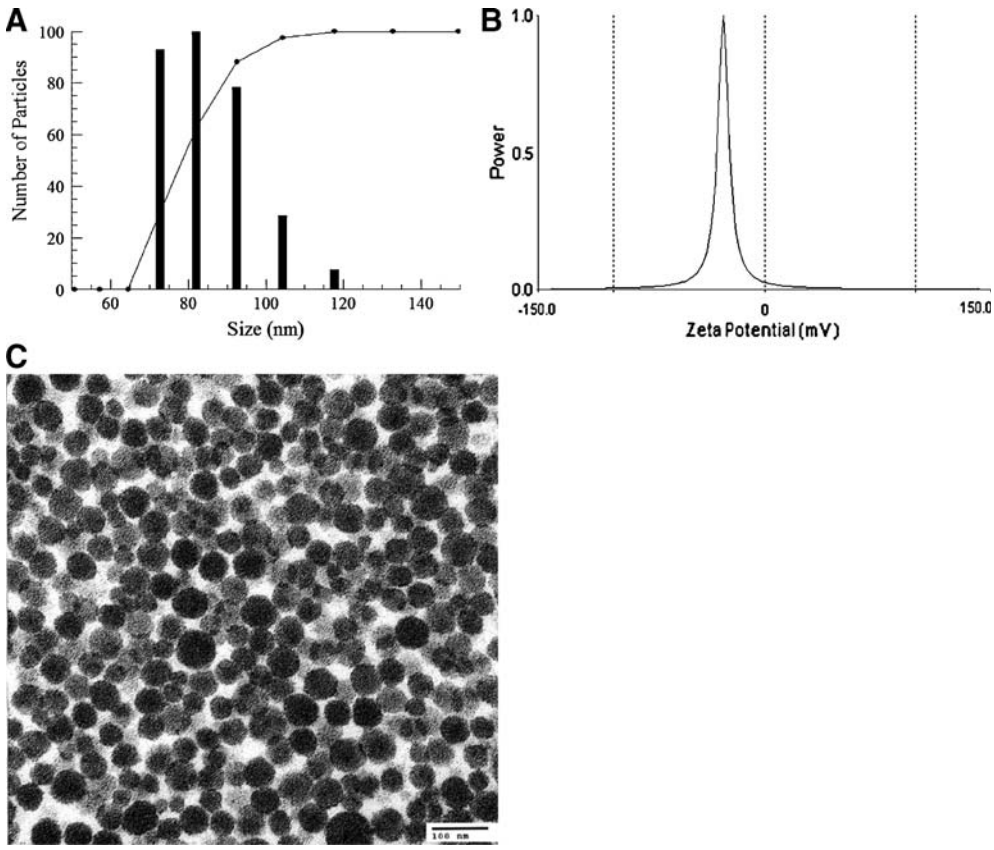

Fig. 1. Particle analysis and electron microscope photograph. The size and surface charge of HSA-NP was 107.3±31.1 nm (**A**) and −23.73±3.03 mV (**B**), respectively. **C** The HSA-NP showed a spherical and uniform shape.

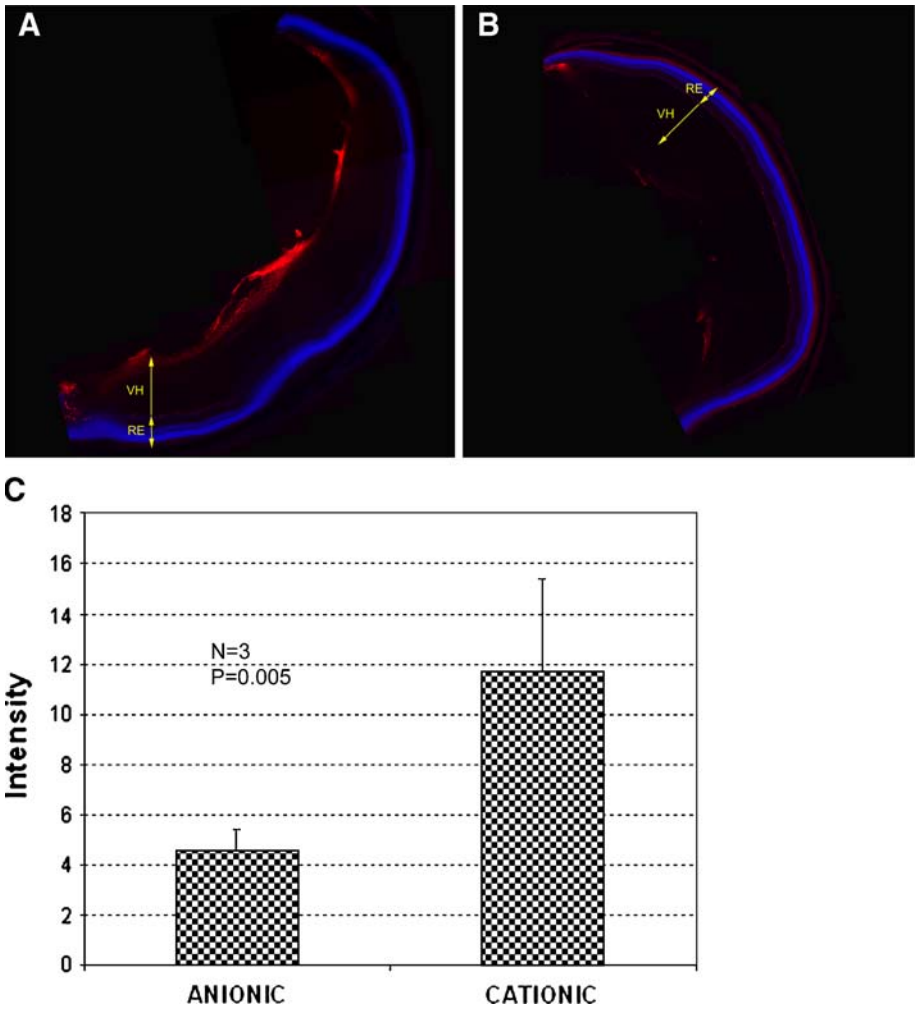

Fig. 2. The vitreal distribution of Alexa 555 conjugated **A** cationic and **B** anionic HSA-NP 5 h post intravitreal administration. **C** The average fluorescence intensity in the vitreous between the anionic and cationic HSA-NP injected eyes. Cell nuclei were stained with DAPI (*blue color*). *RE* = retina; *VH* = vitreous.

Retinal Penetration of HSA-NP

Intravitreally administered anionic HSA-NPs penetrated into the deep retinal structures in both the normal (Fig. 3A, B) and laser photocoagulated retina (Fig. 3C, D). In the laser photocoagulated retina, more HSA-NPs were detected in the choroidal space, compared to the normal retina. In Fig. 3, some HSA-NPs were observed to distribute around the retinal vascular structures. Figure 4 indicates that HSA-NPs could not penetrate the blood retinal barrier. In Fig. 4A, the yellow arrows indicate HSA-NPs at the ab-luminal surface of the retinal vasculature. In Fig. 4B, C, blue, green, grey, and red colors represent the Von Willebrand Factor positive cells (the vascular endothelium), Müller cells, nuclei, and HSA-NPs, respectively. HSA-NPs were located at the ab-luminal side and had not in fact penetrated the retinal vascular barrier.

Retinal Penetration Mechanism of Intravitreal HSA-NPs

Figure 5A shows the distribution of intravitreally administered HSA-NPs in the whole retina 5 h post administration. The distribution of HSA-NPs in the ONL indicates that the particles might penetrate the retinal tissue layers through a specific route (Fig. 5B). Some HSA-NPs were endocytosed and located in the RPE 5 h post intravitreal injection (Fig. 5C).

The HSA-NP and Müller cell co-localization experiment was performed to provide a possible mechanism for HSA-NP retinal penetration. Figure 6A–C shows the distribution of HSA-NPs 5 h post injection, Müller cell immunostaining, and the co-localization, respectively. Most HSA-NPs co-localized with the Müller cells in the inner limiting membrane and ganglion cell layer (Fig. 6D), the inner nuclear layer and outer plexiform layer (Fig. 6F), and the outer nuclear layer (Fig. 6G). However, many HSA-NPs in the inner plexiform layer were not co-localized with the Müller cells (Fig. 6E).

DISCUSSION

The delivery of therapeutic agent-encapsulating nanoparticles into the retina and RPE is promising for the treatment of many severe retinal eye diseases. PLA or PLGA-based nanoparticles have been extensively studied

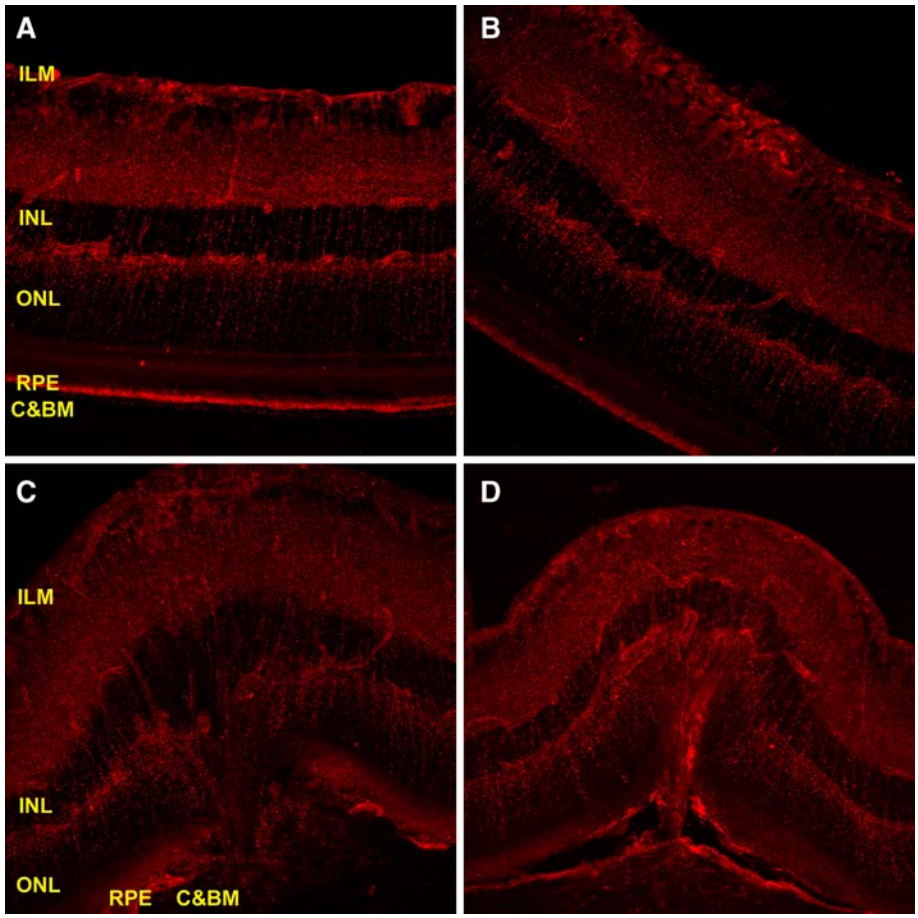

Fig. 3. The retinal distribution of Alexa 555 conjugated anionic HSA-NP in the (**A**, **B**) normal and (**C**, **D**) laser photocoagulated retina. *ILM* = inner limiting membrane; *INL* = inner nuclear layer; *ONL* = outer nuclear layer; *RPE* = retinal pigment epithelium; *C&BM* = choroid and Bruch's membrane.

for intravitreal drug delivery (14–16). Both are biodegradable and biocompatible and have been approved for human use by the US Food and Drug Administration. However, the mild inflammatory reaction after the injection of these polymer-based nanoparticles was observed in the vitreous, retina and ciliary body (15). In this study, we prepared human serum albumin based nanoparticles, which show high encapsulation efficiency of various drugs (7). More importantly, the HSA-NP is a non-immunogenic safe carrier for the intravitreal delivery of drugs.

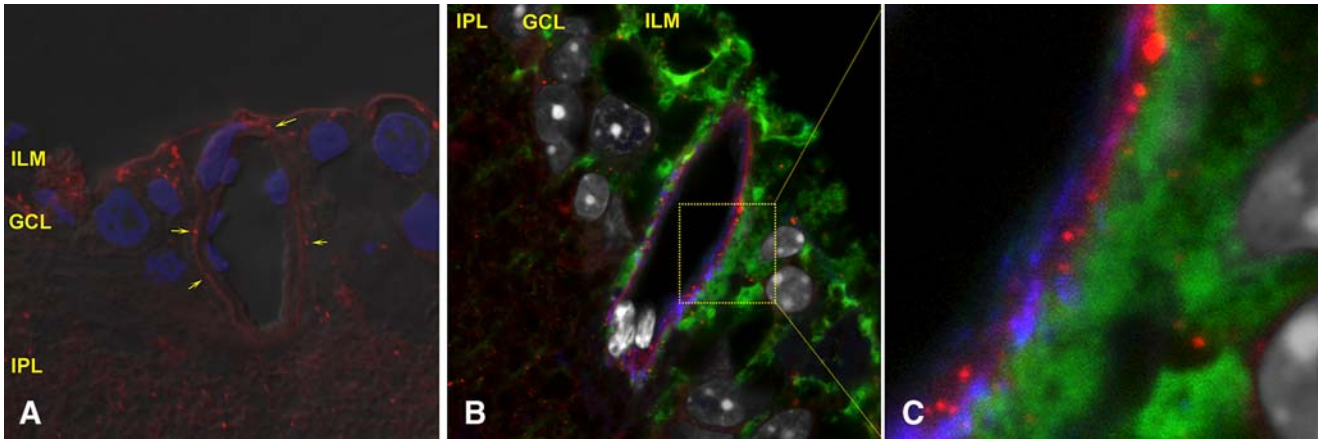

Fig. 4. The distribution of HSA-NPs around the retinal vasculature 5 h post intravitreal administration. **A** The *yellow arrows* localize HSA-NPs at the ab-luminal surface of the retinal vasculature. **B**, **C** The immunohistochemistry staining confirming the ab-luminal distribution of HSA-NPs. *Blue*, *green*, *grey*, and *red* colors represents the Von Willebrand Factor positive cells, Müller cells, Nuclei, and HSA-NPs, respectively. *ILM* = inner limiting membrane; *GCL* = ganglion cell layer; *IPL* = inner plexiform layer.

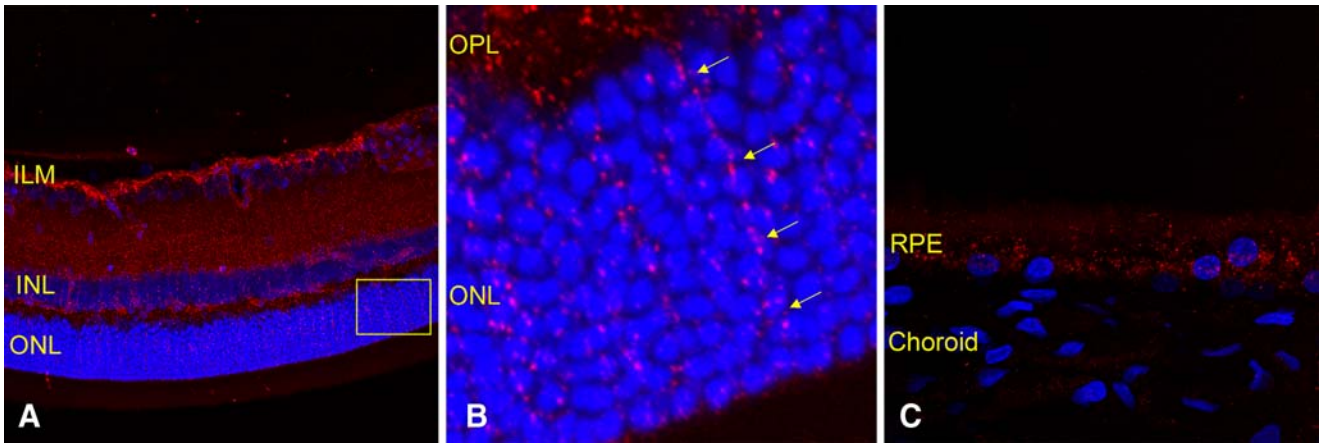

Fig. 5. **A** The distribution of intravitreally administered HSA-NPs in the whole retina 5 h post administration. **B** The rectangular region in **A** was magnified to show the distribution of HSA-NPs in the ONL. **C** The distribution of trans-retinal penetrated HSA-NPs in the RPE 5 h post intravitreal administration. *ILM* = inner limiting membrane; *INL* = inner nuclear layer; *OPL* = outer plexiform layer; *ONL* = outer nuclear layer; *RPE* = retinal pigment epithelium.

A nanoparticle-based ocular drug delivery system can be developed to overcome the vitreal charge and retinal barriers and to deliver therapeutic agents efficiently into the sub-retinal space and RPE, depending on size and charge (6). The vitreous is a well-ordered, three-dimensional network of collagen fibrils bridged by proteoglycan filaments (17). Sakurai *et al.* reported that different sized nanoparticles (2-μm, 200-nm, and 50-nm) diffused in the vitreous (18). Nanoparticles with 2-μm diameter diffused in the vitreous cavity to the trabecular meshwork; while, nanoparticles, whose diameter is smaller than 200 nm, were also observed in the retina and other tissues. Two-micrometer, 200-nm, and 50-nm particles showed different half-lives, 5.4±0.8, 8.6±0.7, and 10.1±1.8 days, respectively. In this study, we investigated the importance of charge on intravitreal nanoparticle movement. The vitreous is composed of water (99%) and colloids (0.1%), with the remainder of the solid material comprised of ions and low-molecular weight solutes (19). The structure of the vitreous is formed by collagen (40–120 μg/mL) and hyaluronic acid (100–400 μg/mL) (19). Vitreal hyaluronan is the most common negatively charged glycosaminoglycan. These glycosaminoglycans are known to interact with polymeric and liposomal DNA complexes (20,21). Peeters *et al.* (21) showed in an *in vitro* study that cationic liposome complexes clearly aggregated in the vitreous. By increasing the degree of pegylation of the liposome and decreasing the zeta potential to become anionic, the author discovered that binding of the liposome to the biopolymers in the vitreous decreased and observed homogeneous spreading of non-aggregated anionic liposome. Our *in vivo* experimental data (Fig. 2) were consistent with the previous *in vitro* findings. Intravitreally administered anionic HSA-NPs diffused freely in the posterior direction from the vitreous to the retina (Fig. 2B). However, most of intravitreally administered cationic HSA-NPs (zeta potential=11.7±7.2 mV) were bound and aggregated to the vitreous (Fig. 2A). Few cationic particles were observed in the retina 5 h post intravitreal administration. One limitation in this study was that human serum albumin was cationized as previously described and then confirmed the cationization in distilled water, not in the vitreous (11,22). Therefore, it is limited to determine the real zeta potential of nanoparticles in the vitreous matrix. The other limitation in the study was that we injected two different size (175 and 114.0 nm) HSA-NPs to compare the vitreal distribution of cationic and anionic HSA-NPs. Since 120-nm PEG coated polystyrene nanoparticles diffused 1.6 fold faster than 182-nm sized ones, 175-nm sized HSA-NPs can be expected to diffuse slower than 114-nm sized ones (21). The difference of vitreal diffusion due to the different diameter might affect the distribution of intravitreal HSA-NP in Fig. 2. However, 250-nm sized HSA-NPs as well as 310-nm sized PLA particles were dispersed in the vitreous (7,15). Therefore, our conclusion, that anionic nanoparticles can diffuse more freely in the vitreous than cationic ones, is still correct. According to the *in vitro* study(19) and our current *in vivo* study, it could be concluded that cationic charge is a more important limiting factor than molecular size on the vitreous mobility of nanoparticles.

The retina is a soft and fragile multilayer structure. Some layers show formidable barriers against the trans-retinal penetration of macromolecules. The inner limiting membrane (ILM) is located between retinal Müller cell end feet and the vitreous cortex and, as such, is a true basement membrane of Müller cells (23). The ILM is composed of a fine three-dimensional meshwork structure with numerous pores whose size ranges from 10 to 25 nm. The pores of the ILM act as the main filtration barrier between the retina and the vitreous cavity (24). Kamei *et al.* reported that intravitreally injected 70 kDa tissue plasminogen activator could not diffuse across the ILM (25). The ILM is composed of several components (23). Some components, hyaluronan, heparin sulfate, chondroitin sulfate, dermatan sulfate, show negative charge (26,27). Accordingly, in addition to being a mechanical barrier, the ILM is an electrostatic barrier. In *in-vitro* studies, Jackson TL *et al.* (28) determined the maximum molecule size able to freely penetrate the retina of pig, cattle, and rabbit to be 60±11.5, 78.5±20.5 and 86±30 kDa, respectively. The inner and outer plexiform layers showed high resistance to the diffusion of macromolecules through the retina. Photoreceptor inner segments and apical processes of Müller cells are connected by a row of *zonulae adherents* that collectively form the external limiting membrane (ELM) (29). The pore

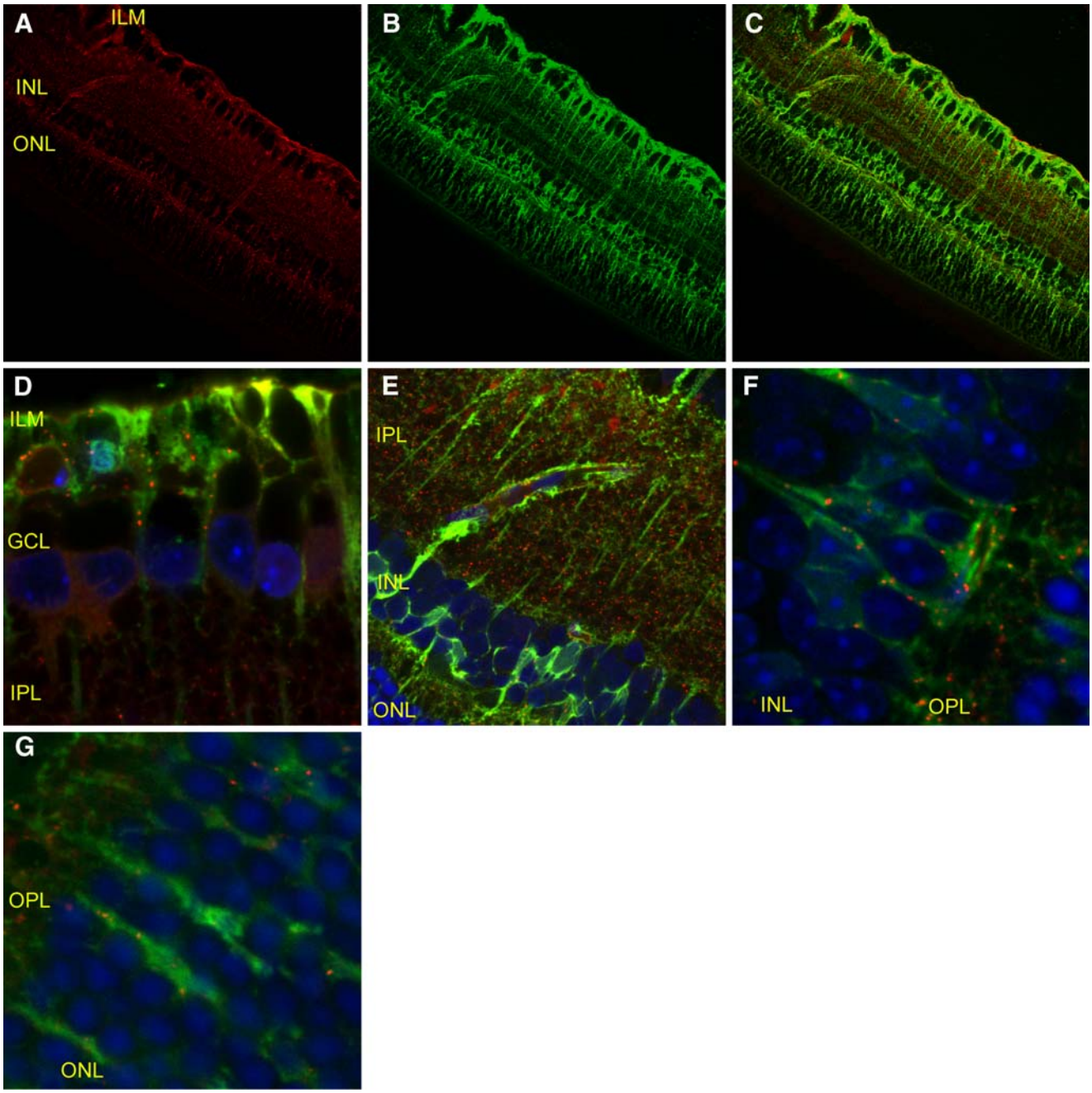

Fig. 6. Co-localization of intravitreally administered HSA-NPs and the Müller cells. **A**–**C** the retinal distribution of HSA-NPs 5 h post injection, Müller cell immunostaining, and the co-localization, respectively. The detailed co-localization is shown in **D** the inner limiting membrane and ganglion cell layer; **E** the inner plexiform layer; **F** the inner nuclear layer and outer plexiform layer; **G** the outer nuclear layer, respectively. *ILM* = inner limiting membrane; *GCL* = ganglion cell layer; *IPL* = inner plexiform layer; *INL* = inner nuclear layer; *OPL* = outer plexiform layer; *ONL* = outer nuclear layer.

radius of the *zonulae adherents* of the ELM is between 30 and 36 Å (29). Albumin did not diffuse through the ELM. Contrary to expectations from previous studies about the trans-retinal penetration of macromolecules, the relatively rapid trans-retinal movement of the nanoparticles with diameters greater than 100 nm was been demonstrated (14–16). The size and charge of nanoparticles had little influence on the intraocular tissue distribution of the sub-350-nm particles (15). In our study, Fig. 3 shows the trans-retinal penetration of HSA-NP into the RPE in normal retina (Fig. 3A, B) and laser coagulated retina (Fig. 3C, D) 5 h post intravitreal injection. Figure 5B indicates trans-retinal penetration of HSA-NP occurs through a specific route. Figure 6D–F showed co-localization of HSA-NPs and the Müller cells in the ILM and ganglion cell layer (Fig. 6D), the inner nuclear layer and outer plexiform layer (Fig. 6E), and the outer nuclear layer (Fig. 6F). Several previous studies reported that nanoparticles penetrate the corneal epithelium through a trans-cellular pathway (30). Additionally, several studies have demonstrated nanoparticles overcome the

blood–brain barrier by endocytosis/transcytosis (31). Normand *et al.* demonstrated that *in vivo*, nano-sized vectosomes injected into the vitreous followed a trans-retinal migration before being rapidly internalized by RPE cells. (32) The retinal course of the vectosome appeared to be associated with Müller glial cell distribution (32). Therefore, it may be concluded from this study that the intravitreal nanoparticles might be endocytosed into the Müller cells at the ILM, diffuse within the intracellular space, and then be exocytosed from the Müller cell at the ELM into the interphotoreceptor matrix.

In the normal retina, the intravitreally injected HSA-NPs penetrated the whole retina and localize inside the RPE (Fig. 3A, B). In our study, we did not observe the penetration of HSA-NPs across the RPE in the normal retina. The laser photocoagulation made the outer nuclear layer extended into the choroid through the disruption site of the RPE and Bruch's membrane (33,34). HSA-NPs were observed to reach the choroid through the disruption site of the RPE and Bruch's membrane (Fig. 3C, D). In wet age-related macular degeneration (AMD), it is demanded to deliver therapeutic agents to the choroid region in order to inhibit choroidal neovascularization. Therefore, the anionic HSA-NP is a promising drug delivery carrier for the treatment of AMD.

ACKNOWLEDGMENTS

The authors thank Robert N. Fariss, Ph.D. for advice in the confocal imaging in the study.

REFERENCES

1. S. Duvvuri, S. Majumdar, and A. K. Mitra. Drug delivery to the retina: challenges and opportunities. *Expert. Opin. Biol. Ther.* **3**:45–56 (2003). doi:10.1517/14712598.3.1.45.
2. D. H. Geroski, and H. F. Edelhauser. Drug delivery for posterior segment eye disease. *Invest. Ophthalmol. Vis. Sci.* **41**:961–964 (2000).
3. J. B. Jonas, I. Kreissig, A. Sofker, and R. F. Degenring. Intravitreal injection of triamcinolone for diffuse diabetic macular edema. *Arch. Ophthalmol.* **121**:57–61 (2003). doi:10.1001/archopht.121.5.729.
4. J. I. Lim, R. A. Wolitz, A. H. Dowling, H. R. Bloom, A. R. Irvine, and D. M. Schwartz. Visual and anatomic outcomes associated with posterior segment complications after ganciclovir implant procedures in patients with AIDS and cytomegalovirus retinitis. *Am. J. Ophthalmol.* **127**:288–293 (1999). doi:10.1016/S0002-9394(98)00443-7.
5. T. S. Shane, and D. F. Martin. Endophthalmitis after ganciclovir implant in patients with AIDS and cytomegalovirus retinitis. *Am. J. Ophthalmol.* **136**:649–654 (2003). doi:10.1016/S0002-9394(03)00333-7.
6. S. K. Sahoo, F. Dilnawaz, and S. Krishnakumar. Nanotechnology in ocular drug delivery. *Drug Discov. Today.* **13**:144–151 (2008). doi:10.1016/j.drudis.2007.10.021.
7. J. M. Irache, M. Merodio, A. Arnedo, M. A. Camapanero, M. Mirshahi, and S. Espuelas. Albumin nanoparticles for the intravitreal delivery of anticytomegaloviral drugs. *Mini. Rev. Med. Chem.* **5**:293–305 (2005).
8. Y. Mo, M. E. Barnett, D. Takemoto, H. Davidson, and U. B. Kompella. Human serum albumin nanoparticles for efficient delivery of Cu, Zn superoxide dismutase gene. *Mol. Vis.* **13**:746–757 (2007).
9. S. Segura, S. Espuelas, M. J. Renedo, and J. M. Irache. Potential of albumin nanoparticles as carriers for interferon gamma. *Drug Dev. Ind. Pharm.* **31**:271–280 (2005).
10. C. Weber, J. Kreuter, and K. Langer. Desolvation process and surface characteristics of HSA-nanoparticles. *Int. J. Pharm.* **196**:197–200 (2000). doi:10.1016/S0378-5173(99)00420-2.
11. D. Fischer, T. Bieber, S. Brusselbach, H. Elsasser, and T. Kissel. Cationized human serum albumin as a non-viral vector system for gene delivery? Characterization of complex formation with plasmid DNA and transfection efficiency. *Int. J. Pharm.* **225**:97–111 (2001). doi:10.1016/S0378-5173(01)00765-7.
12. M. Sehested, and K. Hou-Jensen. Factor VII related antigen as an endothelial cell marker in benign and malignant diseases. *Virchows. Arch. A. Pathol. Anat. Histol.* **391**:217–225 (1981). doi:10.1007/BF00437598.
13. H. Chen, and A. J. Weber. Expression of glial fibrillary acidic protein and glutamine synthetase by Muller cells after optic nerve damage and intravitreal application of brain-derived neurotrophic factor. *Glia.* **38**:115–125 (2002). doi:10.1002/glia.10061.
14. R. A. Bejjani, D. BenEzra, H. Cohen, J. Rieger, C. Andrieu, J. C. Jeanny, G. Gollomb, and F. F. Behar-Cohen. Nanoparticles for gene delivery to retinal pigment epithelial cells. *Mol. Vis.* **11**:124–132 (2005).
15. J. L. Bourges, S. E. Gautier, F. Delie, R. A. Bejjani, J. C. Jeanny, R. Gurny, D. BenEzra, and F. F. Behar-Cohen. Ocular drug delivery targeting the retina and retinal pigment epithelium using polylactide nanoparticles. *Invest. Ophthalmol. Vis. Sci.* **44**:3562–3569 (2003). doi:10.1167/iovs.02-1068.
16. Y. de Kozak, K. Andrieux, H. Villarroya, C. Klein, B. Thillaye-Goldenberg, M. C. Naud, E. Garcia, and P. Couvreur. Intraocular injection of tamoxifen-loaded nanoparticles: a new treatment of experimental autoimmune uveoretinitis. *Eur. J. Immunol.* **34**:3702–3712 (2004). doi:10.1002/eji.200425022.
17. L. I. Los, M. J. van Luyn, and P. Nieuwenhuis. Organization of the rabbit vitreous body: lamellae, Cloquet's channel and a novel structure, the 'alae canalis Cloqueti'. *Exp. Eye. Res.* **69**:343–350 (1999). doi:10.1006/exer.1999.0708.
18. E. Sakurai, H. Ozeki, N. Kunou, and Y. Ogura. Effect of particle size of polymeric nanospheres on intravitreal kinetics. *Ophthalmic. Res.* **33**:31–36 (2001). doi:10.1159/000055638.
19. L. Pitkanen, M. Ruponen, J. Nieminen, and A. Urtti. Vitreous is a barrier in nonviral gene transfer by cationic lipids and polymers. *Pharm. Res.* **20**:576–583 (2003). doi:10.1023/A:1023238530504.
20. M. Ruponen, S. Yla-Herttuala, and A. Urtti. Interactions of polymeric and liposomal gene delivery systems with extracellular glycosaminoglycans: physicochemical and transfection studies. *Biochim. Biophys. Acta.* **1415**:331–341 (1999). doi:10.1016/S0005-2736(98)00199-0.
21. L. Peeters, N. N. Sanders, K. Braeckmans, K. Boussery, J. Van de Voorde, S. C. De Smedt, and J. Demeester. Vitreous: a barrier to nonviral ocular gene therapy. *Invest. Ophthalmol. Vis. Sci.* **46**:3553–3561 (2005). doi:10.1167/iovs.05-0165.
22. W. Lu, Y. Zhang, Y. Z. Tan, K. L. Hu, X. G. Jiang, and S. K. Fu. Cationic albumin-conjugated pegylated nanoparticles as novel drug carrier for brain delivery. *J. Control. Release.* **107**:428–448 (2005). doi:10.1016/j.jconrel.2005.03.027.
23. S. R. Russell, J. D. Shepherd, and G. S. Hageman. Distribution of glycoconjugates in the human retinal internal limiting membrane. *Invest. Ophthalmol. Vis. Sci.* **32**:1986–1995 (1991).
24. H. Nishihara. Studies on the ultrastructure of the inner limiting membrane of the retina—distribution of anionic sites in the inner limiting membrane of the retina. *Nippon. Ganka. Gakkai. Zasshi.* **95**:951–958 (1991).
25. M. Kamei, K. Misono, and H. Lewis. A study of the ability of tissue plasminogen activator to diffuse into the subretinal space after intravitreal injection in rabbits. *Am. J. Ophthalmol.* **128**:739–746 (1999). doi:10.1016/S0002-9394(99)00239-1.
26. L. Chai, and J. E. Morris. Distribution of heparan sulfate proteoglycans in embryonic chicken neural retina and isolated inner limiting membrane. *Curr. Eye Res.* **13**:669–677 (1994). doi:10.3109/02713689408999903.
27. S. Heegaard, O. A. Jensen, and J. U. Prause. Structure and composition of the inner limiting membrane of the retina. SEM on frozen resin-cracked and enzyme-digested retinas of *Macaca mulatta*. *Graefes. Arch. Clin. Exp. Ophthalmol.* **224**:355–360 (1986). doi:10.1007/BF02150029.

28. T. L. Jackson, R. J. Antcliff, J. Hillenkamp, and J. Marshall. Human retinal molecular weight exclusion limit and estimate of species variation. *Invest. Ophthalmol. Vis. Sci.* **44**:2141–2146 (2003). doi:10.1167/iovs.02-1027.
29. A. H. Bunt-Milam, J. C. Saari, I. B. Klock, and G. G. Garwin. Zonulae adherents pore size in the external limiting membrane of the rabbit retina. *Invest. Ophthalmol. Vis. Sci.* **26**:1377–1380 (1985).
30. M. J. Alonso. Nanomedicines for overcoming biological barriers. *Biomed. Pharmacother.* **58**:168–172 (2004). doi:10.1016/j.biopha.2004.01.007.
31. J. Kreuter. Nanoparticulate systems for brain delivery of drugs. *Adv. Drug Deliv. Rev.* **47**:65–81 (2001). doi:10.1016/S0169-409X(00)00122-8.
32. N. Normand, F. Valamanesh, M. Savoldelli, F. Mascarelli, D. BenEzra, Y. Courtois, and F. Behar-Cohen. VP22 light controlled delivery of oligonucleotides to ocular cells *in vitro* and *in vivo*. *Mol. Vis.* **11**:184–191 (2005).
33. T. Fukuchi, K. Takahashi, K. Shou, and M. Matsumura. Optical coherence tomography (OCT) findings in normal retina and laser-induced choroidal neovascularization in rats. *Graefes Arch Clin. Exp. Ophthalmol.* **239**:41–46 (2001). doi:10.1007/s004170000205.
34. R. J. Marano, I. Toth, N. Wimmer, M. Brankov, and P. E. Rakoczy. Dendrimer delivery of an anti-VEGF oligonucleotide into the eye: a long-term study into inhibition of laser-induced CNV, distribution, uptake and toxicity. *Gene. Ther.* **12**:1544–1550 (2005).